Hidden ordered structure in the archetypical Fe(pyrazine)[Pt(CN) 4] spin-crossover porous coordination compound

Ángel Fernández-Blanco, Lorenzo Mariano, Lucía Piñeiro-López, José Antonio Real, Jose Sanchez Costa, Roberta Poloni, J. Alberto Rodríguez-Velamazán

Hidden ordered structure in the archetypical Fe(pyrazine)[Pt(CN)$_4$] spin-crossover porous coordination compound

Ángel Fernández-Blanco,[†,‡] Lorenzo A. Mariano,[‡] Lucía Piñeiro-López,[¶] José Antonio Real,[§] Jose Sanchez Costa,[¶] Roberta Poloni,[*,‡] and J. Alberto Rodríguez-Velamazán[*,†]

†*Institut Laue Langevin, 71 Avenue des Martyrs, CS 20156-38042, Grenoble, France*

‡*Univ. Grenoble Alpes, SIMaP, Grenoble-INP, SIMaP, 38042 Grenoble, France*

¶*IMDEA Nanociencia, Faraday 9, Ciudad Universitaria de Cantoblanco, 28049 Madrid, Spain*

§*Departamento de Química Inorgánica, Insituto de Ciencia Molecular (ICMol), Universidad de Valencia, Spain*

Received May 5, 2022; E-mail: roberta.poloni@grenoble-inp.fr; velamazan@ill.eu

Abstract: Despite the fact that Fe(pyrazine)[M^{II}(CN)$_4$] (where M^{II} is a metal in open square-planar configuration, namely Pt, Pd, Ni) is one of the most thoroughly studied families of spin-crossover compounds, its actual structure has remained imprecisely known up to now. Using neutron diffraction and density-functional theory calculations, we demonstrate that the pyrazine rings, instead of being disordered in two orthogonal positions in the low-spin phase, adopt an ordered arrangement with the rings alternatively oriented in these two positions. This finding has a direct implication on the most characteristic property of these systems, the spin-crossover transition, which is notably affected by this arrangement. This is because the energy difference between both spin states depends on the pyrazine configuration and the ordering of the rings changes the balance of entropy contributions to the entropy-driven spin-crossover phenomenon.

Introduction

Coordination chemistry has experienced a remarkable surge in the last years largely due to the burgeoning of metal-organic frameworks (MOFs), a topic where the structure-property correlation plays a crucial role. Evidently, X-ray diffraction is an essential tool in this research field, but it has some limitations that may be overcome with other techniques. In this line, neutron diffraction is a powerful complement, in particular for cases where hydrogen positioning is important, since it gives information that can be essential, as we illustrate in this work.

A new field opened for spin-crossover (SCO) materials[1] when the bistability provided by the SCO phenomenon was combined with porosity in a porous coordination polymer (PCP) or a MOF.[2] This combination opened a vast playground of possibilities for applications in fields like gas capture[3] or chemical sensing,[4] since SCO can both modulate the interaction with the guest molecule and be modulated by the interaction with an adsorbed molecule.[5–9] An archetypical example of this class of compounds is the family Fe(pyrazine)[M^{II}(CN)$_4$] (where M^{II} is a metal in open square-planar configuration, namely Pt, Pd, Ni).[10,11] Based on the classical Hofmann clathrate compounds,[12] these three-dimensional frameworks present, together with the mentioned combination of porosity and SCO,[13,14] an extremely rich display of functional properties. These include, for example, chemo-[15–17] and photo-switching,[18–20] molecular rotation correlated with the change of spin state,[21] or pressure-tunable bistability.[22] Inspired by this approach, many other examples have followed, aiming at enhancing the porosity,[23] the cooperativity and loading capacity,[24] as well as the interplay between the host-guest function and the SCO.[25] The structure of Fe(pyrazine)[M^{II}(CN)$_4$] adopts a general topology consisting of 2D {Fe[M^{II}(CN)$_4$]}$_\infty$ layers, with the pyrazine ligands occupying the apical positions of the Fe octahedra and connecting the layers along the perpendicular direction (Fig. 1). Three possible configurations can be contemplated for the orientation of the pyrazine rings in a layer (Fig. 1): the molecules in parallel configuration, in perpendicular configuration in two positions at 90° one from each other, or orientationally disordered in these two positions (disordered configuration). It is generally assumed that the pyrazine rings are orientationally disordered, this disorder being dynamic in the high-spin (HS) state and nearly static in the low spin (LS) state.[21] Initially, a tetragonal space group $P4/m$, which implies a disordered configuration due to the 4-fold axis passing through the N atoms of the pyrazine, was proposed from the structural determination based on PXRD data.[10] Later, single-crystal x-ray diffraction studies allowed the assignation of the $P4/mmm$ space group (also implying a disordered configuration),[13,15–17,26] which has been thoroughly assumed in subsequent studies for these compounds in both spin states in absence of host molecules. Interestingly, Southon et *al.*[13] pointed to a parallel configuration upon incorporation of two water molecules per unit cell. They found a twinned structure with orthorhombic space group $Pmmm$, with the pyrazines parallel within each twin, but with 50:50 occupation of both possible orthogonal orientations. In the same work, the authors reported also an intermediate partially dehydrated phase, with one water molecule in the cavities presenting a perpendicular configuration of the pyrazine rings characterized by the appearance of superstructure peaks. The disordered configuration was nevertheless retained for the apohost.

In this work, we use neutron diffraction to demonstrate that the pyrazine rings adopt the perpendicular configuration in the LS state in the guest-free Fe(pyrazine)[Pt^{II}(CN)$_4$] compound, contrarily to what has been generally assumed before. This observation is fully confirmed by density-functional theory calculations performed on the two configurations. Finally, the consequences of the pyrazine ordering on the spin crossover transition temperature are discussed based on the effect on the computed energy and entropy contributions. These findings have important implications

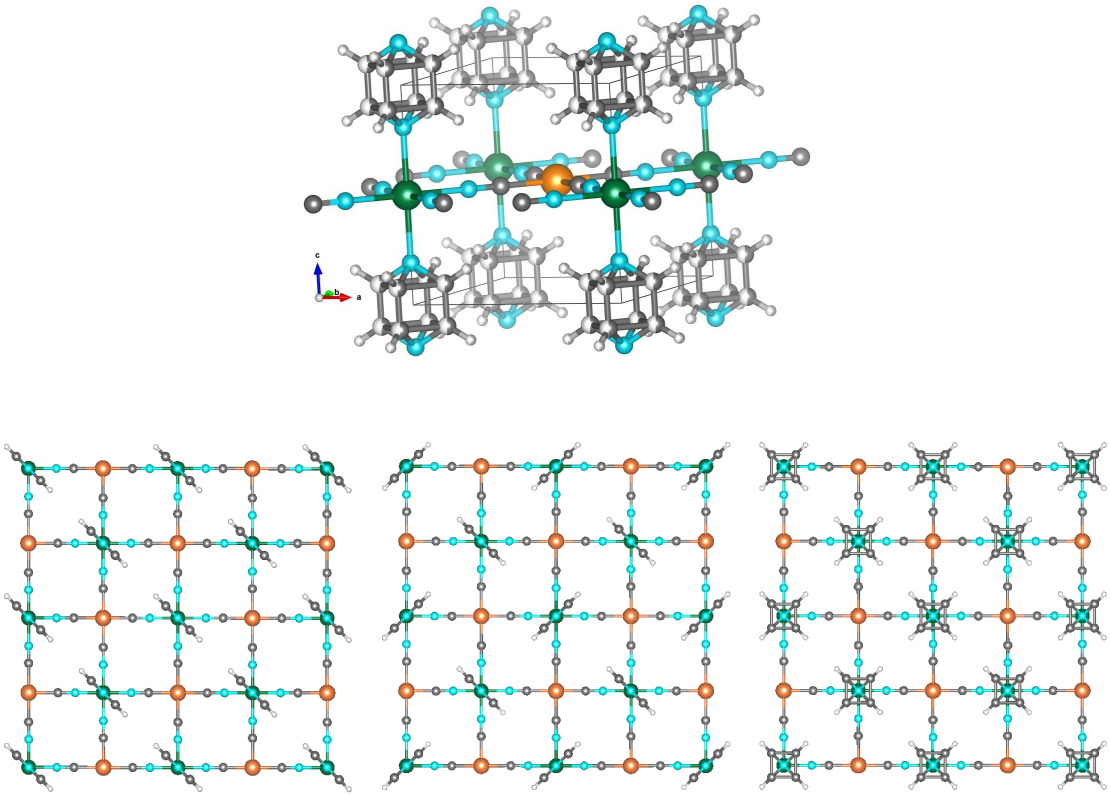

Figure 1. (Top) Scheme of the crystal structure of Fe(pyrazine)[$M^{II}(CN)_4$] with the pyrazine rings in disordered configuration: Fe (green), M^{II} (orange), N (light blue), C (dark grey), H (light grey). The unit cell is represented as black lines. (Bottom) Representations of the three possible configurations of the pyrazine bridges: in parallel configuration, in perpendicular configuration and in disordered configuration.

because the number of studies dedicated to this family is huge owing to the vast panoply of remarkable properties these compounds present.

Results and discussion

Neutron diffraction

The structure of the generally accepted disordered configuration is described in the $P4/mmm$ tetragonal space group with cell parameters $a = b = 7.33(3)$ Å, $c = 6.94(2)$ Å for the low-spin state.[15] The perpendicular configuration implies instead a structural transformation to a tetragonal supercell with $\mathbf{a}'' = \mathbf{a} - \mathbf{b}$, $\mathbf{b}'' = \mathbf{a} + \mathbf{b}$, and $\mathbf{c}'' = \mathbf{c}$, giving $a'' = b'' \approx \sqrt{2}a$ and $c'' \approx c$.[13] This transformation may therefore involve the emergence of superstructure diffraction peaks. However, when working with x-rays, these peaks are weak and can be overlooked, in particular in powder diffraction. Additionally, these superstructure reflections can be diffuse, because the orientation of the rings may be uncorrelated between layers along c.[13] The contrast provided by neutrons for light atoms (like the hydrogen in the pyrazine molecule) allows distinguishing between the possible configurations of the rings, in particular if hydrogen is replaced by the more coherent scatterer deuterium (Fig. 2). We note that the parallel configuration, with the same cell parameters as the disordered configuration, but space group $Pmmm$[15] is also clearly distinguishable when using neutron diffraction on the deuterated compound (Fig. 2).

Dehydrated microcrystalline Fe(pyrazine)[$Pt^{II}(CN)_4$] and its d_4-pyrazine homologue Fe(d_4-pyrazine)[$Pt^{II}(CN)_4$] were prepared as described elsewhere.[10,15–17] Neutron diffraction experiments were performed on powder samples of ca. 0.25 g using the D20 instrument[27] at Institut Laue-Langevin, Grenoble, France, equipped with a cryo-furnace and using a wavelength of 1.54 Å coming from a germanium monochromator. Rietveld refinements and calculations of the structures were performed using the FullProf suite of programs[28,29] and the tools from the Bilbao Crystallographic Server.[30]

The neutron diffraction results are shown in Fig. 3 and Table 1. Fig. 3a shows the neutron diffraction pattern of Fe(d_4-pyrazine)[$M^{II}(CN)_4$] at 100K (low-spin state). At $2\theta = 19.5$, 23.7 and 34.7 degrees, the superstructure reflections appearing due to the pyrazine ordering in perpendicular configuration can be clearly observed. The experimental pattern agrees well with a model with the pyrazine rings in perpendicular configuration, described in the supercell defined above, with a tetragonal space group $P4/mbm$[13] presenting a 4-fold axis passing through the Pt atom. We note that the real symmetry is probably lower, but the tetragonal pseudosymmetry avoids overparametrization. The fit is slightly improved if some disorder is allowed between both perpendicular positions of the pyrazine - with a refined value of 17.4 (3) %. This is consistent with some degree of orientational disorder and with defects in the correlation of the layers along c.

The ordering in perpendicular configuration of the pyrazine bridges is concomitant with the spin transition. The recorded diffraction patterns on cooling from 320 K to 245 K (Fig. 3b) show the appearance of the superstructure re-

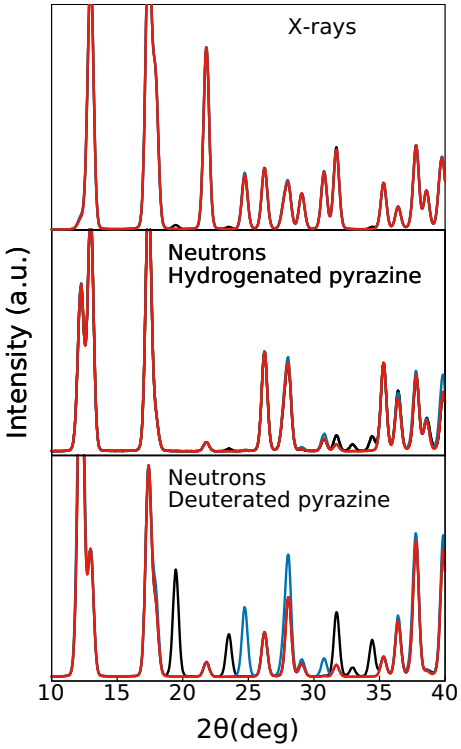

Figure 2. Simulated powder diffraction patterns (wavelength 1.54 Å) of Fe(pyrazine)[$Pt(CN)_4$] in low-spin state with the pyrazine rings in disordered configuration (red lines), in ordered perpendicular (black lines) and parallel (blue lines) configurations: (top) X-rays and hydrogenated pyrazine; (middle) neutrons and hydrogenated pyrazine; (bottom) neutrons and deuterated pyrazine.

flections at the same temperature (ca. 285 K) of the abrupt change in the whole pattern occurring at the transition. The perpendicular configuration is the most stable at low temperatures (see below) and in fact it has been observed in similar compounds not displaying spin-crossover.[31] However, in the present case, it sets up concurrently with the abrupt structural changes produced at the spin transition. It deserves to be noted that the perpendicular configuration is also the one found compatible with the experimental results and calculations when certain types (and quantities) of molecules are adsorbed.[13,32] In the high-spin state, the diffractogram does not show any signal of superstructure reflections and can be satisfactorily fitted with the disordered model with space group $P4/mmm$ (Fig. 3c). It is worthy of note that the ordering of the pyrazine molecules in the low-spin state is not an effect of the deuteration. Indeed, although less visible than in the deuterated compound, the diffraction patterns measured for the hydrogenated compound in the low-spin state (Fig. 3d) also show evidence of pyrazine ordering (see the superstructure reflections at $2\theta = 34.6$ degrees).

Pyrazine interaction

In order to understand the greater stability of the perpendicular configuration we have performed DFT calculations using the Quantum ESPRESSO package.[33,34] The PBE+D2 functional[35,36] was used to compute the binding energy of three different pyrazine dimers that represent the possible configurations present in the system: i) perpendicular, ii) top-on and iii) side-to-side dimers for the parallel arrangement (see inset of Fig. 4). See computational details in the Supporting Material for more details.

Taking the positions and structures of the pyrazine rings from the corresponding relaxed compound as starting point, one of the monomers was moved along the axis that connects the centers of mass of the two molecules until a local minimum was reached. The potential energy curves obtained for the three configurations are represented in Fig. 4. The three minima were found at center-to-center distances ($R_{centers}$) between pyrazines of 4.8 Å, 3.8 Å, and 6.4 Å for the perpendicular, top-on, and side-to-side dimers, respectively. We note that the distance between complexed pyrazines in the framework is 7.1 Å, which is significantly larger than any of these $R_{centers}$ and falls almost at the end of the potential energy curves (see circles on the curves of Fig. 4). An attractive interaction is predicted nonetheless for every configuration at $R_{centers}$=7.1 Å, being E_{int} = -11.1 meV and E_{int} = -6.7 meV for the perpendicular and side-to-side configurations, respectively, and negligible (E_{int} =-0.2 meV) for the top-on dimer. By adding up the side-to-side and the top-on energy contributions we obtain a lower value than the interaction predicted for the perpendicular configuration. This simple dimer model therefore suggests a perpendicular configuration of pyrazines for molecules located at the same distance found in the clathrate.

We note the unusual shape of the potential energy curve of the side-to-side configuration where two different regions can be found: a stabilization region between 6.1 Å and 7.6 Å and a destabilization region for $R_{centers} > 7.6$ Å. The first corresponds to d(H-H) between [2.1 - 3.4] Å which correlates with the typical formation distances of H-H bond.[37,38] This weak bond of dispersive nature exhibits energies of the order of 0.017 eV, comparable to the maximum stabilization of 0.020 eV predicted at the equilibrium position in Fig. 4. For $R_{centers} > 7.6$ Å, the H-H distance is too large for a typical H-H bond and the electrostatic repulsion between the pyrazines may dominate. Finally, this analysis is consistent with the (PBE+D2) computed total energy difference between the parallel and perpendicular configurations in the supercell which gives a more stable perpendicular case by 35 meV per pyrazine.

Influence of the pyrazine arrangement on the spin transition

The configuration of the pyrazine rings has important consequences for the most characteristic feature of this material: the spin-crossover transition. The spin transition temperature, $T_{1/2}$, from LS to HS is defined as the temperature at which the thermodynamic equilibrium between the two phases is reached, i.e. when the Gibbs free energy is zero. The transition temperature is then given by $T_{1/2} = \Delta H_{HS\text{-}LS}/\Delta S_{HS\text{-}LS}$, being $\Delta H_{HS\text{-}LS}$ ($\Delta S_{HS\text{-}LS}$) the enthalpy (entropy) difference between both spin states. The experimental values for these quantities are ΔH_{exp} = 25 kJ mol^{-1} and ΔS_{exp} = 84 J mol^{-1} K^{-1} (giving $T_{1/2}$ = 297 K).[11] Both the energy and the entropy differences depend on the configuration of the pyrazine rings, and therefore the transition temperature would be substantially modified if the pyrazine arrangement were different.

The enthalpy difference, $\Delta H_{HS\text{-}LS}$, contains two terms, the adiabatic energy difference, ΔE_{ad}, and the vibrational contribution, ΔE_{vib}. The entropy variation, $\Delta S_{HS\text{-}LS}$, con-

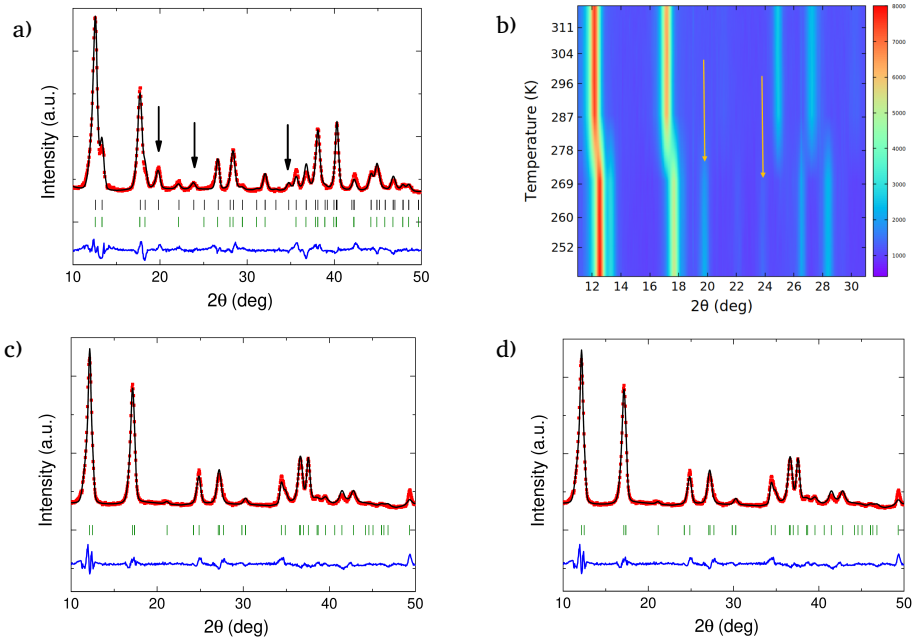

Figure 3. Detail of the most relevant part of the powder neutron diffraction patterns (wavelength 1.54 Å) of Fe(d_4-pyrazine)[$Pt(CN)_4$] (a,c) and Fe(pyrazine)[$Pt(CN)_4$] (d). Experimental patterns (red), calculated (black), and difference patterns (blue lines). Position of the Bragg reflections for the disordered configuration (green marks) and the ordered arrangement of the pyrazine bridges in perpendicular configuration (black marks). The arrows indicate the observed superstructure reflections related with the ordering of the pyrazine bridges in perpendicular configuration. Panel a) Fe(d_4-pyrazine)[$Pt(CN)_4$] in the low-spin state (100 K). Panel b) Neutron thermodiffractograms collected on cooling from 320 K to 245 K (cooling rate ca. 1.5 K/min, acquisition every 5 minutes) for Fe(d_4-pyrazine)[$Pt(CN)_4$]. Panel c) Fe(d_4-pyrazine)[$Pt(CN)_4$] in the high-spin state (320 K). Panel d) Fe(pyrazine)[$Pt(CN)_4$] in the low-spin state (130 K).

Table 1. Results of the refinement of the powder neutron diffraction patterns of Fe(d_4-pyrazine)[$Pt(CN)_4$] and Fe(pyrazine)[$Pt(CN)_4$]: space group, cell parameters, selected distances and agreement factors are reported in each case.

Compound	Fe(d_4-pyrazine)[$Pt(CN)_4$]		Fe(pyrazine)[$Pt(CN)_4$]	
T(K)	100	320	130	320
Spin state	Low-spin	High-spin	Low-spin	High-spin
Space group	$P4/mbm$	$P4/mmm$	$P4/mbm$	$P4/mmm$
a, b (Å)	10.1568(4)	7.4285(8)	10.1576(5)	7.4299(3)
c (Å)	6.7632(5)	7.2316(7)	6.7668(4)	7.2369(5)
$d_{Fe-N(C)}$ (Å)	1.903(5)	2.1599(3)	1.941(5)	2.1583(2)
$d_{Fe-N(pz)}$ (Å)	1.983(7)	2.2273(3)	1.978(7)	2.2291(3)
R_{Bragg}	5.69	7.70	5.03	8.81

tains the vibrational contribution, ΔS_{vib}, a rotational term, ΔS_{rot}, which accounts for the degrees of freedom associated with the rotational motion of the pyrazine rings,[21] plus an electronic contribution, ΔS_{el}, that takes into account the different spin multiplicity between the two spin states. In the case of a LS-HS transition in Fe(II) complexes between a LS state with S = 0 and a HS state with S = 2, ΔS_{el} = 13.38 J mol^{-1} K^{-1}. This term, which represents ca. 16% of the entropy variation at the transition, is independent from the arrangement of the pyrazine rings.

ΔS_{rot} is instead significantly affected by the pyrazine configuration. This term was calculated to amount to 7.95 J mol^{-1} K^{-1} [21] (ca. 9.4% of the total entropy gain at the transition) assuming a LS state with the pyrazine rings disordered in two perpendicular positions. If the pyrazine molecules are ordered in LS, the number of accessible positions is divided by two, and so does the entropy. This would lead to differences in ΔS_{rot} of at least a factor of two (under the approximation used of a harmonic oscillator around its equilibrium position, which is the case with less entropy, and therefore less favorable to produce big differences when applying a factor two to it). A difference of this magnitude in ΔS_{rot} implies a divergence of ca. of 10% of the total entropy.

We performed DFT calculations (see computational details in the Supporting Material) to compute how the pyrazine configuration affects the other terms such as E_{ad}, E_{vib} and S_{vib}. For this we computed total energy and normal modes for the compound with the pyrazine rings in perpendicular and in parallel configuration in both the HS and LS states. We take the average of the perpendicular and parallel cases as an approximation for the disordered case (see the full set of values in Table S1 of the Supporting Information). The expression for the vibrational contributions E_{vib} and S_{vib} can be derived within the statistical thermodynamic theory from the partition function of a harmonic oscillator. For a given normal modes vibrational spectrum $\{\nu_i\}$, the vibrational contributions are:

$$E_{vib} = R \sum_{\nu_i} \frac{h\nu_i}{k_B} \left(\frac{1}{2} + \frac{1}{e^{h\nu_i/k_B T} - 1} \right) \qquad (1)$$

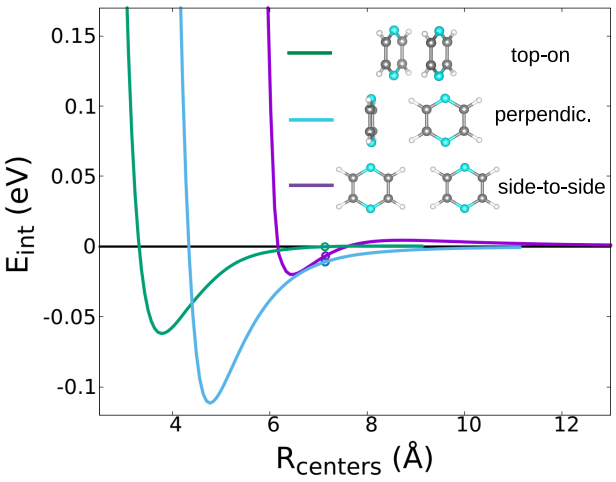

Figure 4. Interaction energy, E_{int}, computed for the three pyrazine dimers: top-on (green), perpendicular (light blue), and side-to-side (purple). The x-axis ($R_{centers}$) gives the center-to-center distance between pyrazine moeities. The circles indicate the distance at which pyrazines are found in the Hofmann clathrate, i.e. $R_{centers}$ = 7.1 Å.

and

$$S_{vib} = R\sum_{\nu_i}\left(\frac{h\nu_i}{k_BT}\frac{1}{e^{(h\nu_i/k_BT)}-1} - \ln\left(1-e^{-h\nu_i/k_BT}\right)\right) \quad (2)$$

The DFT results show a difference of -0.83 J mol^{-1} K^{-1} in ΔS_{vib} (ca. 1% of the total experimental entropy gain at the transition) between a LS-ordered case and a fully disordered scenario. The LS-ordered case consists of the difference between a disordered HS state and an ordered LS state with a perpendicular arrangement. The fully disordered case is the difference in vibrational entropy computed for a disordered configuration both in the HS and LS states. The sign of the difference in this term is opposite to the case of ΔS_{rot}. Regarding ΔE_{vib}, a negligible difference of -0.02 kJ mol^{-1} (less than 0.1% of the total enthalpy variation at the transition) is computed.

Finally, the adiabatic energy difference, ΔE_{ad}, is computed as the total energy difference between the two spin states each taken at its corresponding geometry. We note that the calculation of adiabatic energy differences in transition metal complexes represents a significant challenge for modern electronic structure methods.[39–43] Within DFT, different exchange and correlation functionals including semilocal, meta-GGAs, and global hybrids have been tested in this respect and variations by up to 3 eV can be found depending on the specific choice of the functional and the chosen molecular complex.[44] Here, to evaluate ΔE_{ad}, we use the non-self consistent Hubbard U-corrected density approach scheme which employs linear response U[45] values computed separately for high spin and low spin (see SI for more details). This method has recently been shown to provide accurate results of spin splitting energies for a series of Fe(II) molecules and periodic compounds when compared with higher level calculations and experimentally extracted results.[43] The adiabatic energy difference computed with this method is 36.64 kJ mol^{-1} when both spin states are disordered and 36.91 kJ mol^{-1} when the LS state is in perpendicular arrangement. This gives, as expected, a marginal energy difference of 0.27 kJ mol^{-1} between the two pyrazine configurations.

Adding together all the contributions, we obtain that the change in the configuration of pyrazine moieties in the LS state from disordered to a perpendicular arrangement implies an increase of 0.25 kJ mol^{-1} in ΔH and of ca. 7 J mol^{-1} K^{-1} in ΔS at the spin transition, which translates in a variation of $T_{1/2}$ of the order of 20 K. Thus, if the configuration of the pyrazine rings in the LS state were disordered and not ordered (with the other terms assumed unchanged), the transition temperature would have been *ca.* 20 K lower.

Conclusion

Herein we have demonstrated, by means of neutron diffraction experiments, that the pyrazine rings in Fe(pyrazine)[Pt(CN)$_4$] adopt an ordered arrangement in the low-spin state with the rings alternatively oriented in the two positions perpendicular to each other. Our DFT calculations have shown, one one hand, that this configuration stems from the interaction between the pyrazine molecules and, on the other hand, have allowed us to estimate the effect of this arrangement in the spin transition temperature. The implications of the actual configuration of the pyrazine moieties in the energy and entropy balance between the high-spin and low-spin states are substantial, and thus the spin transition temperature is significantly dependent on this configuration. The fact that Fe(pyrazine)[M^{II}(CN)$_4$] (M^{II} = Pt, Pd, Ni) are prototypical examples of the growing class of porous spin-crossover compounds, with a relevant potential for applications, and the great number of studies concerning this family and many other compounds based on it, underlines the significance of the accurate structural knowledge, which may be of crucial importance for the understandig of the properties of such materials.

Conflicts of interest

There are no conflicts to declare.

Acknowledgements

We thank the ILL for the PhD contract of A. F. B. and for the beamtime allocation under experiment numbers 5-22-795 (doi.ill.fr/10.5291/ILL-DATA.5-22-795) and DIR-274 (doi.ill.fr/10.5291/ILL-DATA.DIR-214). J. S. C. acknowledges funds from the MICINN through the National Research Project (PID2019-111479GB-100), the Ramon y Cajal Research Program (RYC-2014-16866). IMDEA Nanociencia acknowledges support from the 'Severo Ochoa' Programme for Centres of Excellence in R&D (MICINN, Grant CEX2020-001039-S). J. A. R. thanks Grant PID2019-106147GB-I00 funded by MCIN/AEI/10.13039/501100011033. Calculations were performed using resources granted by GENCI under the CINES and TGCC grant numbers A0020907211 and A0110907211. Additionally, the froggy and Dahu platform of the CIMENT infrastructure, which is supported by the Rhone-Alpes region (GRANT CPER07_13 CIRA) and the Equip@Meso project, was employed for the calculations.

References

(1) Gütlich, P.; Goodwin, H. A. *Spin-Crossover in Transition Metal Compounds, Vols. I-III, in Topics in Current Chemistry*; Springer: Berlin, 2004.

(2) Real, J. A.; Andrés, E.; Muñoz, M. C.; Julve, M.; Granier, T.; Bousseksou, A.; Varret, F. Spin Crossover in a Catenane Supramolecular System. *Science* **1995**, *268*, 265–267.

(3) Reed, D. A.; Keitz, B. K.; Oktawiec, J.; Mason, J. A.; Runčevski, T.; Xiao, D. J.; Darago, L. E.; Valentina, V. C.; Bordiga, S.; Long, J. R. A spin transition mechanism for cooperative adsorption in metal–organic frameworks. *Nature* **2017**, *550*, 1476–4687.

(4) Halder, G. J.; Kepert, C. J.; Moubaraki, B.; Murray, K. S.; Cashion, J. D. Guest-Dependent Spin Crossover in a Nanoporous Molecular Framework Material. *Science* **2002**, *298*, 1762–1765.

(5) Bao, X.; Shepherd, H. J.; Salmon, L.; Molnár, G.; Tong, M.-L.; Bousseksou, A. The Effect of an Active Guest on the Spin Crossover Phenomenon. *Angew. Chem. Int. Ed.* **2013**, *52*, 1198–1202.

(6) Ohtani, R.; Hayami, S. Guest-Dependent Spin-Transition Behavior of Porous Coordination Polymers. *Chem. Eur. J.* **2017**, *23*, 2236–2248.

(7) Ni, Z.-P.; Liu, J.-L.; Hoque, M. N.; Liu, W.; Li, J.-Y.; Chen, Y.-C.; Tong, M.-L. Recent advances in guest effects on spin-crossover behavior in Hofmann-type metal-organic frameworks. *Coord. Chem. Rev.* **2017**, *335*, 28–43.

(8) Resines-Urien, E.; Burzurí, E.; Fernandez-Bartolome, E.; García García-Tuñón, M. A.; de la Presa, P.; Poloni, R.; Teat, S. J.; Sanchez Costa, J. A switchable iron-based coordination polymer toward reversible acetonitrile electro-optical readout. *Chem. Sci.* **2019**, *10*, 6612–6616.

(9) Develioglu, A.; Resines-Urien, E.; Poloni, R.; Martín-Pérez, L.; Sanchez Costa, J.; Burzurí, E. Tunable Proton Conductivity and Color in a Nonporous Coordination Polymer via Lattice Accommodation to Small Molecules. *Adv. Sci.* **2021**, *8*, 2102619.

(10) Niel, V.; Martínez-Agudo, J. M.; Muñoz, M. C.; Gaspar, A. B.; Real, J. A. Cooperative Spin Crossover Behavior in Cyanide-Bridged Fe(II)M(II) Bimetallic 3D Hofmann-like Networks (M = Ni, Pd, and Pt). *Inorg. Chem.* **2001**, *40*, 3838–3839, PMID: 11466039.

(11) Tayagaki, T.; Galet, A.; Molnár, G.; Muñoz, M. C.; Zwick, A.; Tanaka, K.; Real, J.-A.; Bousseksou, A. Metal Dilution Effects on the Spin-Crossover Properties of the Three-Dimensional Coordination Polymer Fe(pyrazine)[Pt(CN)$_4$]. *J. Phys. Chem. B* **2005**, *109*, 14859–14867, PMID: 16852882.

(12) Hofmann, K. A.; Küspert, F. Verbindungen von Kohlenwasserstoffen mit Metallsalzen. *Z. Anorg. Chem.* **1897**, *15*, 204–207.

(13) Southon, P. D.; Liu, L.; Fellows, E. A.; Price, D. J.; Halder, G. J.; Chapman, K. W.; Moubaraki, B.; Murray, K. S.; Létard, J.-F.; Kepert, C. J. Dynamic Interplay between Spin-Crossover and HostGuest Function in a Nanoporous MetalOrganic Framework Material. *J. Am. Chem. Soc.* **2009**, *131*, 10998–11009, PMID: 19621892.

(14) Muñoz, M. C.; Real, J. A. Thermo-, piezo-, photo- and chemo-switchable spin crossover iron(II)-metallocyanate based coordination polymers. *Coord. Chem. Rev.* **2011**, *255*, 2068–2093, Special Issue: 39th International Conference on Coordination Chemistry.

(15) Ohba, M.; Yoneda, K.; Agustí, G.; Muñoz, M. C.; Gaspar, A.; Real, J. A.; Yamasaki, M.; Ando, H.; Nakao, Y.; Sakaki, S.; Kitagawa, S. Bidirectional Chemo-Switching of Spin State in a Microporous Framework. *Angew. Chem. Int. Ed.* **2009**, *48*, 4767–4771.

(16) Agustí, G.; Ohtani, R.; Yoneda, K.; Gaspar, A.; Ohba, M.; Sánchez-Royo, J.; Muñoz, M. C.; Kitagawa, S.; Real, J. Oxidative Addition of Halogens on Open Metal Sites in a Microporous Spin-Crossover Coordination Polymer. *Angew. Chem. Int. Ed.* **2009**, *48*, 8944–8947.

(17) Ohtani, R.; Yoneda, K.; Furukawa, S.; Horike, N.; Kitagawa, S.; Gaspar, A. B.; Muñoz, M. C.; Real, J. A.; Ohba, M. Precise Control and Consecutive Modulation of Spin Transition Temperature Using Chemical Migration in Porous Coordination Polymers. *J. Am. Chem. Soc.* **2011**, *133*, 8600–8605, PMID: 21526852.

(18) Bonhommeau, S.; Molnár, G.; Galet, A.; Zwick, A.; Real, J.-A. R.; McGarvey, J. J.; Bousseksou, A. One Shot Laser Pulse Induced Reversible Spin Transition in the Spin-Crossover Complex [Fe(C$_4$H$_4$N$_2$)Pt(CN)$_4$] at Room Temperature. *Angew. Chem. Int. Ed.* **2005**, *44*, 4069–4073.

(19) Cobo, S.; Ostrovskii, D.; Bonhommeau, S.; Vendier, L.; Molnár, G.; Salmon, L.; Tanaka, K.; Bousseksou, A. Single-Laser-Shot-Induced Complete Bidirectional Spin Transition at Room Temperature in Single Crystals of (Fe^{II}(pyrazine)(Pt(CN)$_4$)). *J. Am. Chem. Soc.* **2008**, *130*, 9019–9024, PMID: 18570417.

(20) Castro, M.; Roubeau, O.; Piñeiro López, L.; Real, J. A.; Rodríguez-Velamazán, J. A. Pulsed-Laser Switching in the Bistability Domain of a Cooperative Spin Crossover Compound: A Critical Study through Calorimetry. *J. Phys. Chem. C* **2015**, *119*, 17334–17343.

(21) Rodríguez-Velamazán, J. A.; González, M. A.; Real, J. A.; Castro, M.; Muñoz, M. C.; Gaspar, A. B.; Ohtani, R.; Ohba, M.; Yoneda, K.; Hijikata, Y.; Yanai, N.; Mizuno, M.; Ando, H.; Kitagawa, S. A Switchable Molecular Rotator: Neutron Spectroscopy Study on a Polymeric Spin-Crossover Compound. *J. Am. Chem. Soc.* **2012**, *134*, 5083–5089, PMID: 22364147.

(22) Galet, A.; Gaspar, A.; Muñoz, M. C.; Bukin, G.; Levchenko, G.; Real, J. Tunable Bistability in a Three-Dimensional Spin-Crossover Sensory- and Memory-Functional Material. *Adv. Mater.* **2005**, *17*, 2949–2953.

(23) Bartual-Murgui, C.; Ortega-Villar, N. A.; Shepherd, H. J.; Muñoz, M. C.; Salmon, L.; Molnár, G.; Bousseksou, A.; Real, J. A. Enhanced porosity in a new 3D Hofmann-like network exhibiting humidity sensitive cooperative spin transitions at room temperature. *J. Mater. Chem.* **2011**, *21*, 7217–7222.

(24) Piñeiro López, L.; Seredyuk, M.; Muñoz, M. C.; Real., J. A. Two- and one-step cooperative spin transitions in Hofmann-like clathrates with enhanced loading capacity. *Chem. Commun.* **2014**, *50*, 1833–1835.

(25) Meneses-Sánchez, M.; Turo-Cortés, R.; Bartual-Murgui, C.; da Silva, I.; Muñoz, M. C.; Real, J. A. Enhanced Interplay between Host–Guest and Spin-Crossover Properties through the Introduction of an N Heteroatom in 2D Hofmann Clathrates. *Inorg. Chem.* **2021**, *60*, 11866–11877, PMID: 34347471.

(26) Cobo, S.; Ostrovskii, D.; Bonhommeau, S.; Vendier, L.; Molnár, G.; Salmon, L.; Tanaka, K.; Bousseksou, A. Single-Laser-Shot-Induced Complete Bidirectional Spin Transition at Room Temperature in Single Crystals of (Fe^{II}(pyrazine)(Pt(CN)$_4$)). *J. Am. Chem. Soc.* **2008**, *130*, 9019–9024, PMID: 18570417.

(27) Hansen, T. C.; Henry, P. F.; Fischer, H. E.; Torregrossa, J.; Convert, P. The D20 instrument at the ILL: a versatile high-intensity two-axis neutron diffractometer. *Meas. Sci. Technol.* **2008**, *19*, 034001.

(28) Rodríguez-Carvajal, J. Recent advances in magnetic structure determination by neutron powder diffraction. *Phys. B: Condens. Matter* **1993**, *192*, 55–69.

(29) `http://www.ill.eu/sites/fullprof/`.

(30) Aroyo, M. I.; Perez-Mato, J. M.; Capillas, C.; Kroumova, E.; Ivantchev, S.; Madariaga, G.; Kirov, A.; Wondratschek, H. Bilbao Crystallographic Server: I. Databases and crystallographic computing programs. *Z. Kristallogr. Cryst. Mater.* **2006**, *221*, 15–27.

(31) Rodríguez-Hernández, J.; Lemus-Santana, A.; Ortiz-López, J.; Jiménez-Sandoval, S.; Reguera, E. Low temperature structural transformation in T[Ni(CN)$_4$]·xpyz with x=1,2; T=Mn,Co,Ni,Zn,Cd; pyz=pyrazine. *J. Solid State Chem.* **2010**, *183*, 105–113.

(32) Fernández-Blanco, A.; Piñeiro López, L.; Jiménez-Ruiz, M.; Rols, S.; Real, J.; Rodríguez-Velamazán, J.; Poloni., R. Probing the SO2 Adsorption Mechanism in Hofmann Clathrates via Inelastic Neutron Scattering and Density Functional Theory calculations. *J. Phys. Chem. B* **2022**,

(33) Giannozzi, P. et al. Advanced capabilities for materials modelling with Quantum ESPRESSO. *J. Phys.: Condens. Matter* **2017**, *29*, 465901.

(34) Giannozzi, P.; Baseggio, O.; Bonfá, P.; Brunato, D.; Car, R.; Carnimeo, I.; Carvazzoni, C.; de Gironcoli, S.; Delugas, P.; Ruffino, F. F.; Ferreti, A.; Mazari, N.; Timrov, I.; Urru, A.; Baroni, S. QUANTUM ESPRESSO toward the exascale. *J. Chem. Phys.* **2020**, *152*, 154105–1 – 154105–11.

(35) Grimme, S. Semiempirical GGA-type density functional constructed with a long-range dispersion correction. *J. Comput. Chem.* **2006**, *27*, 1787–1799.

(36) Grimme, S.; Hansen, A.; Brandenburg, J. G.; Bannwarth, C. Dispersion-Corrected Mean-Field Electronic Structure Methods. *Chem. Rev.* **2016**, *116*, 5105–5154.

(37) Grabowski, S. J. *Hydrogen Bonding- New Insights*; 2006.

(38) Wolstenholme, D. J.; Cameron, T. S. Comparative Study of Weak Interactions in Molecular Crystals: HH Bonds vs Hydrogen Bonds. *J. Phys. Chem. A* **2006**, *110*, 8970–8978, PMID: 16836461.

(39) Radoń, M. Benchmarking quantum chemistry methods for spin-state energetics of iron complexes against quantitative experimental data. *Phys. Chem. Chem. Phys.* **2019**, *21*, 4854–4870.

(40) Daku, L. M. L.; Vargas, A.; Hauser, A.; Fouqueau, A.; Casida, M. E. Assessment of Density Functionals for the High-Spin/Low-Spin Energy Difference in the Low-Spin Iron(II) Tris(2, 2'-bipyridine) Complex. *ChemPhysChem* **2005**, *6*, 1393–1410.

(41) Pierloot, K. Transition Metals Compounds: Outstanding Challenges for Multiconfigurational Methods. *Int. J. Quantum Chem.* **2011**, *111*, 3291–3301.

(42) Droghetti, A.; Alfè, D.; Sanvito, S. Assessment of Density Functional Theory for Iron(II) Molecules Across the Spin-Crossover Transition. *J. Chem. Phys.* **2012**, *137*, 124303.

(43) Mariano, L. A.; Vlaisavljevich, B.; Poloni, R. Improved Spin-State Energy Differences of Fe(II) Molecular and Crystalline Complexes via the Hubbard U-Corrected Density. *J. Chem. Theory Comput.* **2021**, *17*, 2807–2816.

(44) Mariano, L. A.; Vlaisavljevich, B.; Poloni, R. Biased Spin-State Energetics of Fe(II) Molecular Complexes within Density-Functional Theory and the Linear-Response Hubbard U Correction. *J. Chem. Theory Comput.* **2020**, *16*, 6755–6762.

(45) Cococcioni, M.; De Gironcoli, S. Linear Response Approach to the Calculation of the Effective Interaction Parameters in the

LDA+U Method. *Phys. Rev. B* **2005**, *71*, 035105.